TlCl:Be,I: A High Sensitivity Scintillation and Cherenkov Radiator for TOF-PET

Nicolaus Kratochwil, *Member, IEEE*, Nathaniel Kaneshige, Giulia Terragni, *Student Member, IEEE*, Roberto Cala, Jared Schott, Edgar van Loef, Lakshmi Soundara Pandian, Emilie Roncali, *Senior Member, IEEE*, Jaroslaw Glodo, Etiennette Auffray, *Member, IEEE*, and Gerard Ariño-Estrada, *Member, IEEE*

***Abstract*—The material requirements for gamma-ray detectors for medical imaging applications are multifold and sensitivity is often overlooked. High effective atomic number (Z_{eff}) Cherenkov radiators have raised the attention in the community due to their potential for harvesting prompt photons. A material with one of the highest Z_{eff} and thus short gamma-ray attenuation length is thallium chloride (TlCl). By doping TlCl with beryllium (Be) or iodine (I), it becomes a scintillator and therefore produces scintillation photons upon gamma-ray interaction on the top of the prompt Cherenkov luminescence. The scintillation response of TlCl:Be,I is investigated in terms of intensity, energy resolution, kinetics, and timing capability with and without energy discrimination. The ratio of prompt to slow scintillation photons is used to derive the intrinsic number of produced Cherenkov photons and compared with analytic calculations avoiding complex Monte Carlo simulations. The experimentally determined number of Cherenkov photons upon 511 keV gamma excitation of 17.9 ± 4.6 photons is in line with our simple calculations yielding 14.5 photons. We observe three scintillation decay time components with an effective decay time of 60 ns. The scintillation light yield of 0.9 ph/keV is sufficient to discriminate events with low energy deposition in the crystal which is used to improve the measured coincidence time resolution from 360-ps FWHM without energy selection down to 235-ps after energy discrimination and time walk correction for 2.8-mm thick TlCl:Be,I crystals, and from 580 to 402 ps for 15.2-mm thick ones. Already with the first generation of doped TlCl encouraging timing capability close to other materials with lower effective atomic number has been achieved.**

***Index Terms*—Cherenkov emission, coincidence time resolution (CTR), TlCl:Be,I, time-of-flight positron emission tomography (TOF-PET).**

Received 3 July 2024; revised 10 September 2024 and 16 October 2024; accepted 22 October 2024. Date of publication 31 October 2024; date of current version 5 March 2025. This work was supported in part by (PI Ariño-Estrada) under Grant NIH R01 EB034062 and (PI Glodo) under Grant NIH 44 EB031656, and in part by the Frame of the Crystal Clear Collaboration at CERN. The work of Giulia Terragni was supported by the Federal Ministry of Education, Science and Research of Austria. *(Corresponding author: Nicolaus Kratochwil.)*

This work did not involve human subjects or animals in its research.

Nicolaus Kratochwil was with the Experimental Physics Department, EP-CMX, European Organization for Nuclear Research, 1217 Meyrin, Switzerland. He is now with the Department of Biomedical Engineering, University of California at Davis, Davis, CA 95616 USA (e-mail: nkratochwil@ucdavis.edu).

Nathaniel Kaneshige was with Radiation Monitoring Devices Inc., Waterdown, MA 02472 USA. He is now with Helion, Everett, WA 98203 USA.

Giulia Terragni is with the Experimental Physics Department, EP-CMX, European Organization for Nuclear Research, 1217 Meyrin, Switzerland, and also with the Technical University of Vienna, 1040 Vienna, Austria.

Roberto Cala was with the Experimental Physics Department, EP-CMX, European Organization for Nuclear Research, 1217 Meyrin, Switzerland, and also with the Departimetno di Fisica, University of Milano-Bicocca, 20126 Milano, Italy.

Jared Schott, Edgar van Loef, Lakshmi Soundara Pandian, and Jaroslaw Glodo are with Radiation Monitoring Devices Inc., Waterdown, MA 02472 USA.

Emilie Roncali is with the Department of Biomedical Engineering and the Department of Radiology, University of California at Davis, Davis, CA 95616 USA.

Etiennette Auffray is with the Experimental Physics Department, EP-CMX, European Organization for Nuclear Research, 1217 Meyrin, Switzerland.

Gerard Ariño-Estrada is with the Department of Biomedical Engineering, University of California at Davis, Davis, CA 95616 USA, and also with the Institut de Física d'Altes Energies, Barcelona Institute of Science and Technology, 08028 Barcelona, Spain.

Color versions of one or more figures in this article are available at https://doi.org/10.1109/TRPMS.2024.3487359.

Digital Object Identifier 10.1109/TRPMS.2024.3487359

I. Introduction

THERE is an increasing interest to use Cherenkov emission for medical imaging, such as time-of-flight positron emission tomography (TOF-PET) [1], [2], [3], [4], [5], [6], or prompt gamma imaging (PGI) [7], [8], [9]. The production of Cherenkov photons depends mostly on the refractive index and the transparency of the material, which allows to consider so far overlooked or new crystal materials. When surveying possible candidates for future medical imaging detectors, several competing requirements need to be considered, such as stopping power, material cost, and timing and energy resolution (ER).

Thallium chloride (TlCl [10], $Z_{eff} = 76$) is one of the encouraging materials and competes with lead fluoride (PbF_2, $Z_{eff} = 77$) for the highest effective atomic number, while having higher effective atomic number than bismuth germanate ($Bi_4Ge_3O_{12}$, $Z_{eff} = 72$) or lutetium oxyorthosilicate (Lu_2SiO_5, $Z_{eff} = 64$) [11]. The gamma-ray attenuation length as function of the energy for TlCl as well as BGO and LSO is displayed in Fig. 1.

The disadvantage of some materials (PbF_2, TlCl, and thallium bromide) is the lack of supporting scintillation response, which complicates the determination of the energy deposition [10], [13], [14], [15] and also leads to a sensitivity drop if no Cherenkov photon is detected [13]. We have tackled this potential weakness of TlCl by the introduction of doping, leading to the production of scintillation photons on the top of the prompt Cherenkov photon signal.

In this work, the luminescence response of TlCl:Be,I upon gamma-ray excitation is investigated in terms of spectral

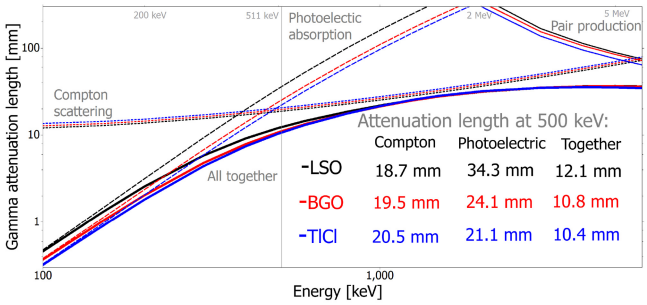

Fig. 1. Gamma-ray attenuation length as function of the energy for LSO (black), BGO (red), and TlCl (blue) for Compton scattering (dotted lines), photoelectric absorption (dashed lines), pair production at higher energies (thin solid lines), and all types of interactions combined (thick solid lines). The inset table shows the attenuation length at 500 keV. Calculations of LSO and TlCl were performed ignoring the small amount of doping with other materials as it hardly impacts the attenuation length. Data is extracted using the NIST database [12].

response, photon yield, kinetics, and achievable coincidence time resolution (CTR) when coupled to silicon photomultipliers (SiPMs).

II. Materials and Methods

A. TlCl Crystals

TlCl:Be,I ingots were grown at RMD using the Bridgman method. The raw materials were purchased from Sigma-Aldrich with 0.9999 purity or greater. Samples with different dimensions were cut from the boules and optically polished. Table I summarizes the properties of the used crystals with pictures shown in Fig. 2.

Light yield (LY) measurements were conducted with the undoped sample (T15), a reference polished BGO pixel purchased from OST Photonics (B11), and a doped TlCl pixel (T1). The latter was also used to study the scintillation kinetics. Transmission and radioluminescence emission spectra were obtained using the cylindrical (T34) sample. After confirming the feasibility to use scintillation light for energy discrimination, two pairs of crystals (T24–T27) were prepared with more favourable geometry (better crystal surface state and edges, smaller cross section) and directly glued to SiPMs for time resolution measurements.

TABLE I
Overview of Crystals Used in This Study

ID	Material	Geometry [mm^3]	Comment
T15	TlCl	≈ 2.8 x 3.0 x 4.8	used in [10], [14]
T1	TlCl:Be,I	≈ 3.2 x 3.7 x 3.8	irregular shape
T34	TlCl:Be,I	⌀9 x 10.6	cylinder
T24	TlCl:Be,I	2.8 x 2.8 x 2.8	encapsulated
T25	TlCl:Be,I	2.8 x 2.8 x 2.8	encapsulated
T26	TlCl:Be,I	2.8 x 2.8 x 15.2	encapsulated
T27	TlCl:Be,I	2.8 x 2.8 x 15.2	encapsulated
B11	BGO	3.0 x 3.0 x 3.0	purchased

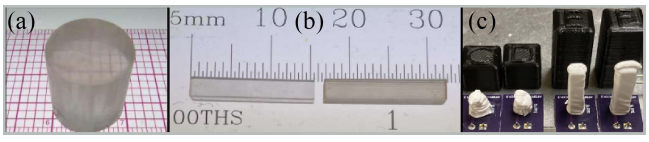

Fig. 2. (a) Picture of the TlCl:Be,I ingot. (b) 15.2-mm thick crystals (T26/T27) before (right) and after (left) polishing. (c) TlCl crystals glued to the SiPMs and wrapped in Teflon before encapsulation (T24–T27).

B. Experimental Setups

1) Transmission Measurement: An Agilent Cary 60 Spectrometer was used to provide a light source between 190 to 900 nm as well as a photodetector to measure the transmission of the sample. The transmission data was calibrated, first by measuring without any sample mounted (100% transmission) and again with the photodetector blocked (0% transmission). The theoretical loss due to double Fresnel reflections (r) expressed in (1) at the boundary between air (refractive index $n_1 = 1.0$) and the crystal and air again amounts to about 30% at 430 nm due to the high refractive index of TlCl of $n_2 = 2.42$

$$r = \left| \frac{n_1 - n_2}{n_1 + n_2} \right|^2. \tag{1}$$

2) Radioluminescence Emission: The radio-luminescence spectrum was measured by placing the crystal in a lead-lined, dark testing enclosure, and exciting the sample with X-rays from a Philips X-ray generator. Upon excitation, the light was then passed through a MCPherson 2-m scanning monochromator, and the monochromator dispersed light was detected using a Burle C31034 photomultiplier tube, cooled using dry ice. The collection time for each wavelength step was 1 s with a measurement range between 200 and 900 nm.

3) Light Yield Measurements: The TlCl crystals and BGO were wrapped in several layers of Teflon and glued with Cargille Meltmount ($n = 1.582$) to a S14160-3050HS SiPM from Hamamatsu (3×3 mm^2 active area and 50 μm cell size), biased at 44 V (+6 V overvoltage). The SiPM signal was amplified with custom readout electronics [16], [17] and the raw waveforms were digitized with an oscilloscope (Tektronix MSO 64B). Measurements were conducted with a ^{22}Na or ^{137}Cs radioactive source placed 5 cm away from the crystal. Additionally, one measurement was performed without any radioactive source with the signal coming solely from SiPM dark counts and correlated crosstalk.

4) Time Correlated Single Photon Counting Measurements: The scintillation kinetics was measured by means of time correlated single photon counting (TCSPC) [18], either with X-ray or with gamma-ray excitation.

Gamma-Ray Excitation: A ^{22}Na source was placed between a fast reference detector and a crystal under test. The detection of a 511 keV gamma-ray in the reference detector was used as the start signal. The TlCl:Be,I sample under test was placed on the top of a SiPM, which is used to measure the light output from the material and thus the deposited energy. The stop signal was given by a photon avalanche diode (ID-Quantique, IDQ). By histogramming the time difference between start and stop signal, upon energy selection, the underlying photon time emission profile was reproduced. Details on the method and setup are given in [19].

X-Ray Excitation: A pulsed laser was used to trigger the production of X-rays in an X-ray tube (Hamamatsu N5084)

with a mean energy of 15 keV (median around 9 keV and maximum energy 40 keV) which excited the TlCl:Be,I sample. A hybrid photomultiplier tube (HPMT) was used to detect the scintillation photons. The coincidence time difference between start and stop signal was plotted to reproduce the underlying scintillation kinetics. Details on the setup are given in [20].

The scintillation time profile was mathematically modeled with a multicomponent bi-exponential function. Data was fitted convolving the function with the impulse response function (IRF) of the respective setup (which was either the contribution of the laser pulse width together with the X-ray time profile and with the HPMT time resolution or the contribution of the reference detector and the single photon time resolution of the IDQ). A Dirac delta function (approximated as a very narrow Gaussian function smaller than the IRF) was added to the rising edge of the bi-exponential scintillation time profile upon gamma-ray excitation to accurately account for Cherenkov emission and to determine the ratio between prompt and scintillation light [3], [19], [21]. The uncertainty was derived by repeating the fit procedure several times with variable starting parameters.

5) Coincidence Time Resolution Measurement: Time resolution was measured with the TlCl:Be,I samples optically coupled (Norland Optical Adhesive 88, $n = 1.56$) to Broadcom NUV-HD SiPMs (AFBR-S4N33C013, 3×3 mm^2 active area, 30-μm cell size, and 37 V bias voltage = 9 V overvoltage) and wrapped with several layers of Teflon. Additionally, the samples were encapsulated to avoid possible surface deterioration due to high UV exposure or moisture. For the measurement, a ^{22}Na source was placed in between the crystals to produce two 511-keV gamma-rays in coincidence.

The voltage drop between SiPM anode and cathode following the detection of light was split and amplified with custom high frequency readout electronics with a balun transformer and two cascade radio frequency amplifiers to generate a steep signal rise time together with low electronic noise [16]. The second branch of the signal was amplified (with an operational amplifier AD 8000) to monitor the total deposited energy via signal integration. The signals were digitized with a LeCroy oscilloscope (DDA 735Zi, 3.5 GHz, and 20 Gs/s) with a coincidence trigger capturing events where the signal passes the threshold of at least five fired cells by both SiPMs. The time pick-off was performed via leading edge discrimination on the oscilloscope, using in-build sin(x)/x interpolation. In addition, the signal rise time between two fixed thresholds (10 and 50 mV) was recorded to perform time walk classification and correction [4]. The measured coincidence time delay distribution was modeled with a sum of two Gaussian fit functions expressed in (2), in line with the previous work exploring Cherenkov emission for fast timing [11], [16]

$$f_{(t)} = \frac{N}{\sqrt{2\pi}} \cdot \left[\frac{r_1}{\sigma_1} \cdot \exp\left(-\frac{(t-\mu)^2}{2\sigma_1^2} \right) + \frac{1-r_2}{\sigma_2} \cdot \exp\left(-\frac{(t-\mu)^2}{2\sigma_2^2} \right) \right]. \tag{2}$$

Hereby N expresses the total number of coincidence events, σ_1 (σ_2) is the standard deviation of the first (second) Gaussian, r_1 is the abundance of the first Gaussian (with $r_2 = 1 - r_1$), and μ is the centroid of the distribution. Uncertainties were estimated by altering the energy window and by analyzing subsets of the data.

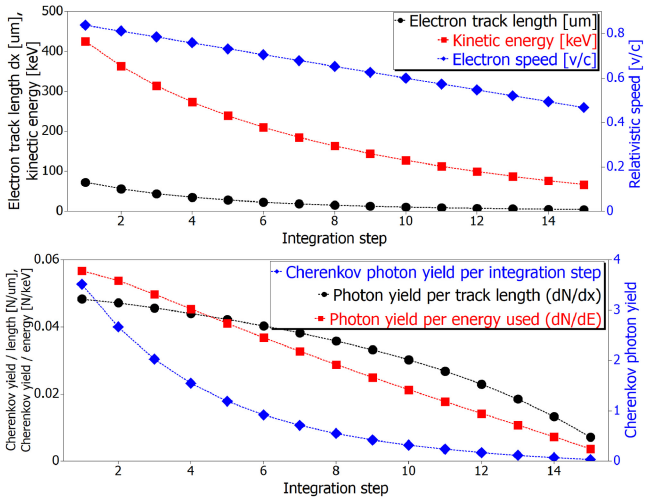

Fig. 3. Top: Electron track length dx, kinetic energy and electron speed as function of the integration step number. Bottom: Produced Cherenkov photons N and differential Cherenkov photon production (dN/dx and dN/dE) for different integration step number. Points are connected as eye-guide.

C. Analytic Calculation of the Cherenkov Photon Production

The intrinsic number of produced Cherenkov photons upon gamma-ray interaction was calculated using the Frank–Tamm (3) [22], [23], with λ being the wavelength, $\beta = (v/c)$ is the speed of the electron, α is the fine structure constant, n is the refractive index, and $z = 1$ is the charge of the electron

$$\frac{d^2N}{dx\,d\lambda} = \frac{2\pi\alpha z^2}{\lambda^2}\left(1 - \frac{1}{\beta^2 n^2(\lambda)}\right). \tag{3}$$

Integration over $d\lambda$ was performed in steps of 1 nm between the cutoff wavelength of 395 and 900 nm. The refractive index follows the dispersion relationship provided by [24] (defined between 430 to 660 nm) and was extrapolated toward 395 nm ($n = 2.54$) and 900 nm ($n = 2.19$). The initial energy of the hot-recoil electron was calculated as 511 keV minus the K-shell binding energy of thallium, resulting in an initial energy of $E_{\text{start}} = 425.5$ keV. This energy corresponds to an electron speed of $\beta_{\text{start}} = 0.84$. The cutoff speed β_{stop}, which is the speed threshold when the electron does not emit Cherenkov light, varies between $\beta_{\text{stop}}(\lambda = 395\text{ nm}) = 0.39$ and $\beta_{\text{stop}}(\lambda = 900\text{ nm}) = 0.46$. Since the speed decreases for increasing path length, an updated speed was used for each dx integration step using the continuous-slowing-down approximation provided by the ESTAR database [25]. For this the values between 10 and 550 keV were extracted and the trend modeled with a third degree polynomial function to calculate any values in between. To simplify calculations, the electron speed was linearly divided from the start speed to the cutoff speed and a variable path length dx was used for each integration, as illustrated on the top of Fig. 3.

The Cherenkov production per electron track length (dN/dx) is almost constant for the first few integration steps shown at the bottom of Fig. 3, indicating that the dx integration size is sufficiently small.

III. Results

A. Spectroscopic Performance

Fig. 4 shows the measured scintillation emission profile of TlCl:Be,I. The peak emission is at 430 nm with a tail down to 600 nm. The Cherenkov emission follows roughly a $1/\lambda^2$ distribution with more photons produced at lower wavelengths.

Fig. 5 shows the measured signal area of TlCl:Be,I (T1) and the undoped sample (T15), when coupled to a SiPM and excited with different gamma-ray sources.

The peak around 700 units corresponds to SiPM dark counts. Two different peaks can be identified when comparing the ^{137}Cs and ^{22}Na excitation which come from the 511 and 662 keV gamma-ray lines with full energy deposition. We see a tail extending toward 3000 units, coming from Compton interactions of the 1.275 MeV gamma-ray line. No scintillation can be observed for undoped TlCl, however we see a small tail which could be due to detection of Cherenkov light.

B. Light Yield Estimation

The light output measurement was repeated with a thin BGO crystal (B11) under the same condition, which yielded the photopeak position for 662 keV gamma-ray excitation at 23.4 ± 0.4 k units. We considered an LY of $LY_{BGO} = 10.7 \pm 1.1$ ph/keV [3] and a weighted detection efficiency of $PDE_{BGO} = 0.44 \pm 0.02$ and $PDE_{TlCl} = 0.47 \pm 0.02$, respectively [26]. The difference in refractive indices between the two materials was also accounted for by using light transfer efficiency (LTE) values of $LTE_{BGO} = 0.65 \pm 0.01$ and $LTE_{TlCl} = 0.625 \pm 0.01$ (assuming a perfectly polished cube-like crystal wrapped in Teflon and coupled with Meltmount to the SiPM, values derived from simulations [14]). The crystal surface area of the TlCl:Be,I crystal was slightly larger (11.8 ± 0.3 mm^2) than the active area of the SiPM (9 mm^2), meaning only a fraction of the light escaping the crystal was detected. The estimated LY of TlCl:Be,I was calculated accounting for the aforementioned corrections and according to (4) with a 662 keV peak position of 1.5 ± 0.1 k units

$$\frac{LY_{\text{TlCl:Be,I}}}{LY_{\text{BGO}}} = \frac{1.5\text{k}}{23.4\text{k}} \cdot \frac{0.47}{0.44} \cdot \frac{0.625}{0.65} \cdot \frac{11.8\ \text{mm}^2}{9\ \text{mm}^2}$$
$$\Rightarrow LY_{\text{TlCl:Be,I}} = 0.92\ \pm 0.18\ \text{ph/keV}. \quad (4)$$

The uncertainty of this measurement was estimated to be 20% based on error propagation and the nonperfect crystal shape. The four main drivers for such high uncertainty were the absolute LY of BGO, the irregular cube-like shape without clean edges of this TlCl crystal, the known impact of the crystal geometry [27], [28], and crystal surface state [14], [29], [30]. The ER at 662 keV is about 50 ± 5% in TlCl:Be,I, which is worse than BGO (ER_{BGO} = 14.5 ± 0.5%). The relative worse ER does not come as a surprise given the low light output and scales with the statistical contribution (ER $\approx 1/\sqrt{LY}$).

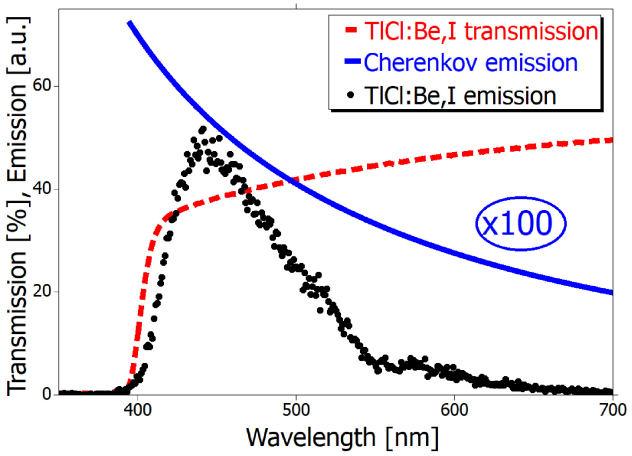

Fig. 4. TlCl:Be,I scintillation and Cherenkov emission spectrum and measured transmission. The Cherenkov emission is amplified by 100 for better visibility and obtained by integrating (3) over *dx*.

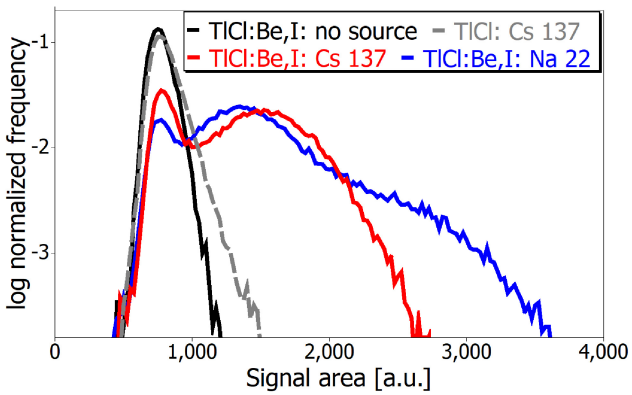

Fig. 5. Measured signal area of TlCl(:Be,I) upon gamma-ray excitation.

C. Scintillation Kinetics

Scintillation kinetics are shown in Fig. 6 for X-ray excitation (left) and gamma-ray excitation (right). Three decay times were observed for both excitation energies with the fastest one $\tau_{d1} = 3.0 \pm 0.3$ ns (2.5% abundance), a medium one of $\tau_{d2} = 50 \pm 4$ ns (33% abundance), and a slow one of $\tau_{d3} = 300 \pm 40$ ns yielding an effective decay time (harmonic average: $1/\tau_{d,eff} = \sum_i R_i/\tau_{d,i}$) for both cases of $\tau_{d,eff} = 60 \pm 3$ ns. The measurement with low energy X-rays eliminated any influence of Cherenkov photons on the scintillation rise time. The scintillation rise time τ_r was below the resolution of the system and the photon time spread in the crystal, which acts in a similar way as the scintillation rise time [3], [31], might be the dominant contribution.

D. Cherenkov Photon Yield

Zooming in on the first few nanoseconds of the TCSPC measurement upon gamma-ray excitation on the left of Fig. 7, one can observe a prompt peak which is due to the detection of Cherenkov photons with a relative abundance of 3.09 ± 0.31%. Using the abundance of this prompt luminescence component and the estimated scintillation LY, we can estimate the number of generated Cherenkov photons upon 511 keV gamma-ray excitation [3]. Since the spectral response of scintillation and Cherenkov emission are different, the abundance needs to be corrected based on the weighted photon detection probability (PDP) of the IDQ between 395

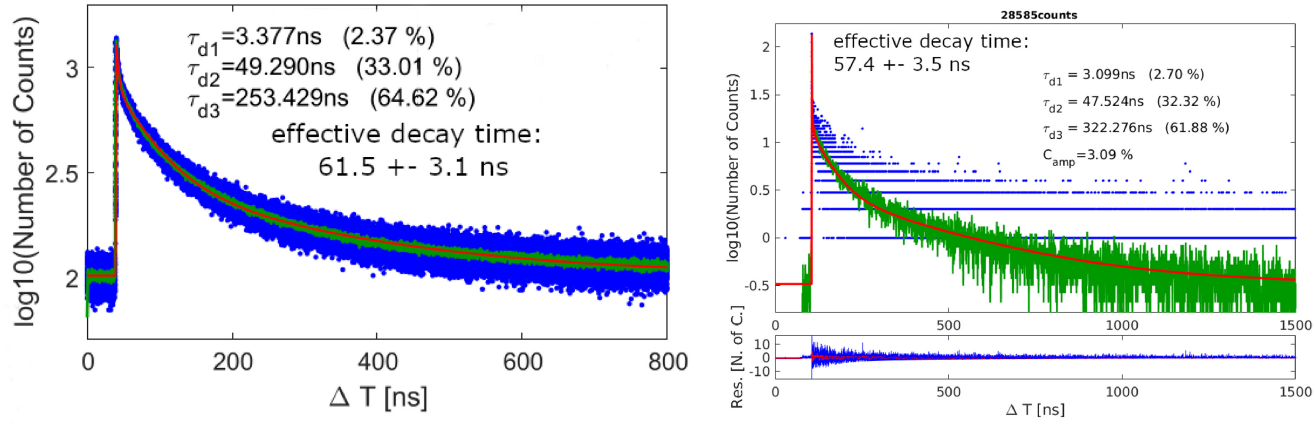

Fig. 6. Scintillation kinetics upon X-ray excitation (left) with median energy of 9 and 511 keV gamma-ray excitation (right). The blue points represent the raw data, green is the moving average for better eye-guidance, and in red is the fit function. The decay time components with the abundance are inserted. The individual values are interconnected with each other and have a precision of about 10%.

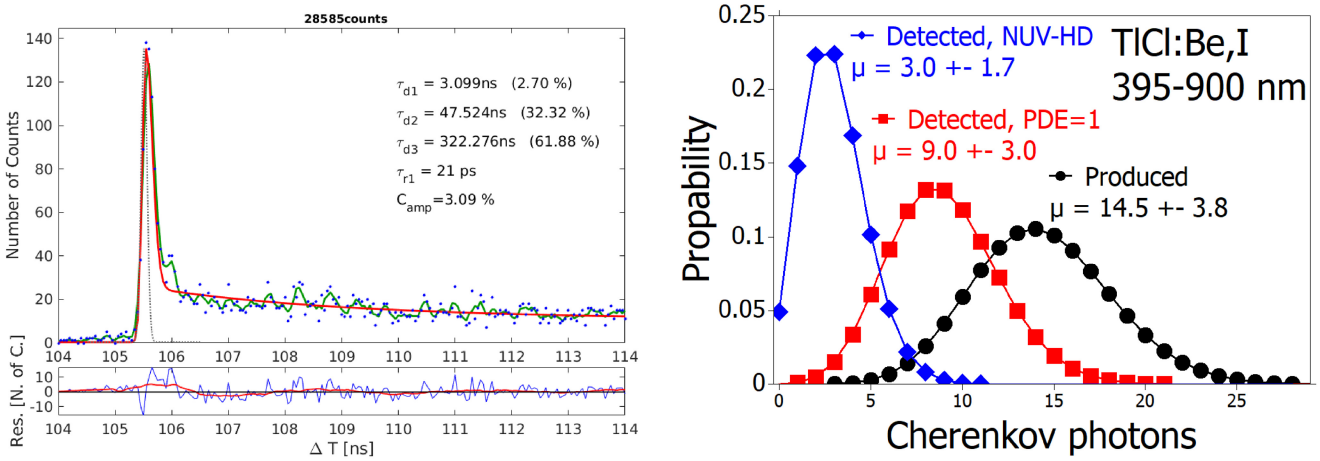

Fig. 7. Left: Zoom-in on the rising part of the TCSPC measurement upon gamma-ray excitation with blue being the raw data, green the moving average and in red the fit function. The abundance of the prompt peak was approximately 3%, the measured scintillation rise time was smaller than the precision of the setup ($\tau_r \leq 30$ ps). Right: Calculated number of Cherenkov photons using the Frank–Tamm equation for TlCl and assuming a Poisson-like distribution. Values are given on the number of produced photons (black), detected photons for a small cube-like crystal wrapped in Teflon and coupled to a SiPM with perfect PDE (red), and considering the detection efficiency of the NUV-HD technology provided by the data-sheet [32] (blue). The uncertainties are calculated as the square root of the variance from the Poisson distribution.

and 900 nm for the scintillation emission ($\text{PDP}_{\text{scintillation}} = 29\%$) and Cherenkov emission ($\text{PDP}_{\text{Cherenkov}} = 23.5\%$). The number of Cherenkov photons N_{Cher} produced in TlCl:Be,I was then calculated according to

$$N_{\text{Cher}} = 0.92 \text{ ph/keV} \cdot 3.09\ \% \cdot \frac{29\ \%}{23.5\ \%} \cdot 511 \text{ keV}$$
$$N_{\text{Cher}} = 17.9\ \pm\ 4.6 \text{ photons}. \quad (5)$$

There are several uncertainties on this experimental Cherenkov photon yield. First, the detection efficiency of the stop detector was only measured up to 800 nm. Linearly extrapolating the PDP up to 900 nm gives an relative error of approximately 8%. Next, the prompt abundance of the fit fluctuates when repeating the fit procedure with different initialization parameters, yielding to an estimated error of 10%. While the scintillation yield is linear with lower energy deposition, the Cherenkov photon yield strongly (nonlinear) depends on the energy of the initial hot-recoil electron, as visible in the dN/dE graph in Fig. 3. While we performed energy discrimination to select photopeak events, with the limited ER, low energy deposition events were not fully discarded, giving an additional 10% error. Finally, the 20% uncertainty of the LY estimation needs to be included as well. Assuming all the described effects are independent, the total uncertainty is 26%, giving an absolute error of 4.6 photons on the estimation. On the right of Fig. 7 the analytically calculated number of Cherenkov photons in TlCl is displayed with an underlying Poisson-like distribution around the mean value, validating the experimental assessment.

E. Coincidence Time Resolution

The CTR of two pairs of TlCl:Be,I crystals was measured. The first pair of crystals (T24, T25: 2.8 × 2.8 × 2.8 mm^3) was used to obtain a time measurement with a minimal contribution from light transport and depth-of-interaction (DOI). The second pair (T27, T28: 2.8 × 2.8 × 15.2 mm^3) was

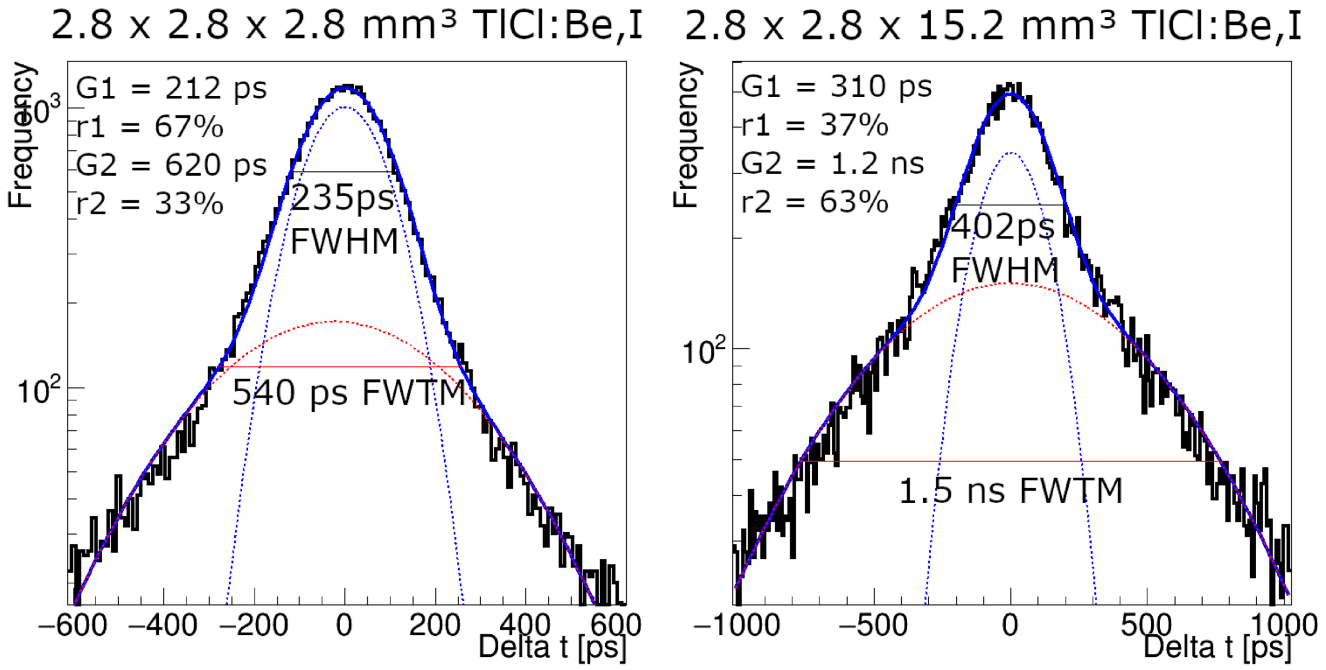

Fig. 8. Measured coincidence time delay histogram (black) in semi-logarithmic scale for pairs of thin (left, T24, T25) and thick (right, T26, T27) TlCl:Be,I. The blue solid line displays the overall distribution, while the dotted lines show the individual Gaussian distribution from (2). The FWHM ($G_{1,2}$) and the relative abundance ($r_{1,2}$) of the individual distributions are stated on the top left of the figures.

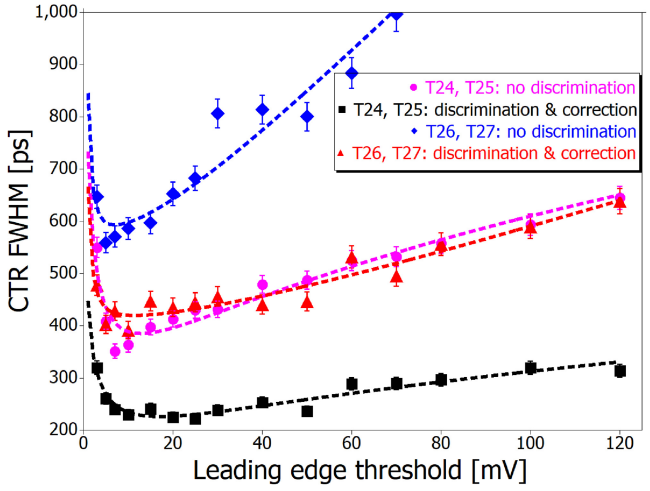

Fig. 9. Measured CTR for pairs of 2.8 × 2.8 × 2.8 mm^3 (T24, T25) and 2.8 × 2.8 × 15.2 mm^3 (T26, T27) TlCl:Be,I crystals in coincidence as function of the leading edge threshold.

used to obtain a measurement of the performance of TlCl crystals with comparable stopping power to those used by commercially available PET systems. Fig. 8 shows the coincidence time delay distribution in a semi-logarithmic scale for the two pairs of TlCl:Be,I crystals measured in coincidence after energy selection and time walk correction. The time resolution as function of the leading edge threshold before and after energy discrimination/time walk correction is shown in Fig. 9. The data was fitted with the function $CTR_{(\mathrm{Thr})} = \sqrt{a_0^n + (a_1 \cdot \mathrm{Thr})^n + (a_2/\mathrm{Thr})^n}$. Without any energy discrimination, the best achievable CTR was 361 ± 5 and 580 ± 7 ps for the pairs of thin and thick crystals, respectively, with a strong dependency on the leading edge threshold in both cases. These values improve to 272 ± 4 and 450 ± 6 ps FWHM after selecting only events with full 511 keV energy deposition and further down to 235 ± 4 and 402 ± 6 ps after time walk correction based on the SiPM signal rise time [4].

IV. Discussion

This manuscript presents the performance evaluation of the first generation of doped TlCl crystals with Be and iodine. The capability to utilize both scintillation and Cherenkov light makes TlCl an encouraging material for various applications where good time resolution and high stopping power are required, such as TOF-PET [33] or PGI [7], [8]. While the ER obtained is lower than well known crystals used in PET, such as BGO and L(Y)SO, the scintillation mechanism allows for a coarse energy discrimination that is not possible with Cherenkov light alone. Moreover, the measured scintillation decay time with fast components of ≈3 and ≈50 ns (60 ns effective decay time) can lead to competitive timing performance, especially with improvements of doping compositions which increase the LY.

The experimental estimation of the Cherenkov photon yield is very well in agreement with the analytic calculation, yielding a mean number of 14.5 Cherenkov photons upon 511 keV gamma-ray excitation (or an electron with initial kinetic energy of 425.5 keV being fully stopped in TlCl). On average only about nine Cherenkov photons reach the photodetector for thin crystals and, given the weighted SiPM detection efficiency, about three Cherenkov photons are detected. This weak Cherenkov response becomes also visible when looking at the shape of the distribution in Fig. 5, as there is a tail for the undoped TlCl sample upon ^{137}Cs excitation with respect to the TlCl:Be,I measurement without any source suggesting the detection of Cherenkov light.

Comparing the timing performance between the thin and thick pair of crystals, we noticed a time resolution degradation. The higher aspect ratio of the crystal reduces the number of photons reaching the SiPM [27], [28], which is particularly severe given the low number of produced Cherenkov photons. Additionally, having only one or two Cherenkov photons detected, those prompt photons might first propagate away from the SiPM before reaching the crystal end and being reflected and later detected, strongly worsening the achievable timing performance due to enhanced photon time spread [11]. One path to mitigate this enhanced photon time spread is dual-ended SiPM readout [34], [35], which is subject for future work. Other options could be side readout [36], or sharing small amounts of the scintillation light laterally with neighboring photodetectors in a crystal array configuration with different reflectors [37], [38].

The measured $\approx$ 400 ps CTR for 15.2 mm thick TlCl:Be,I crystal needs to be viewed considering the crystal properties and stopping power of TlCl: 15.2 mm thick TlCl achieves the same probability for 500 keV gamma-ray photoelectric interaction as a 17.4-mm thick BGO crystal; or a 24.7 mm thick LSO crystal, stressing the importance of the high effective atomic number of TlCl (see Fig. 1). No significant time resolution degradation due to the presence of scintillation light was observed with respect to our previous work with undoped TlCl crystals [10], [11], [14], [39], which confirms the presence of scintillation light does not significantly worsen the timing capability and possible deterioration is compensated by selection on full energy deposition events. The choice of photodetector and readout electronics seems to be more correlated. Furthermore, the achievable CTR for thin TlCl:Be,I of 235 ps FWHM is comparable to the results obtained for BGO of similar geometry coupled to SiPMs from Hamamatsu Photonics (S13360 series) of 237 $\pm$7 ps and slightly worse using the same SiPM technology (Broadcom NUV-HD, CTR = 181 $\pm$4 ps) [27]. This mild timing degradation is expected, given the lower average number of detected Cherenkov photons of TlCl (3 photons) with respect to BGO (4.3 photons) and worse energy discrimination capability.

V. Conclusion and Outlook

Scintillation and Cherenkov luminescence of doped TlCl:Be,I have been studied. While the timing capability of undoped TlCl have been investigated in the past, it is the first time that scintillation photons were used for energy discrimination to improve the timing capability. There is potential for further improvement, for instance an optimization in the doping scheme to accelerate the scintillation kinetics and increase the scintillation efficiency would enhance both CTR and ER. As next steps we foresee measurements in a dual-ended readout configuration to improve the timing capability of thick crystal elements.

Acknowledgment

The datasets used and or analyzed during the current study are available from the corresponding author on reasonable request. The authors declare the following financial interests/personal relationships which may be considered as potential competing interests with the work reported in this paper: Nathaniel Kaneshige, Jared Schott, Edgar van Loef, Lakshmi Soundara Pandian and Jaroslaw Glodo are employed by RMD Inc. All authors declare that they have no known conflict of interest in terms of competing for financial interest or personal relationship that could have an influence or are relevant to the work reported in this paper. All authors gave their approval for the final version of the manuscript.

References

[1] R. Dolenec, S. Korpar, P. Križan, R. Pestotnik, and N. Verdel, "The performance of silicon photomultipliers in cherenkov TOF PET," *IEEE Trans. Nucl. Sci.*, vol. 63, no. 5, pp. 2478–2481, Oct. 2016.

[2] R. Ota et al., "Coincidence time resolution of 30 ps FWHM using a pair of cherenkov-radiator-integrated MCP-PMTs," *Phys. Med. Biol.*, vol. 64, Mar. 2019, Art. no. 7LT01. [Online]. Available: https://dx.doi.org/10.1088/1361-6560/ab0fce

[3] S. Gundacker et al., "Experimental time resolution limits of modern SiPMs and TOF-PET detectors exploring different scintillators and cherenkov emission," *Phys. Med. Biol.*, vol. 65, no. 2, Jan. 2020, Art. no. 25001. [Online]. Available: https://dx.doi.org/10.1088/1361-6560/ab63b4

[4] N. Kratochwil, S. Gundacker, P. Lecoq, and E. Auffray, "Pushing cherenkov PET with BGO via coincidence time resolution classification and correction," *Phys. Med. Biol.*, vol. 65, no. 11, Jun. 2020, Art. no. 115004. [Online]. Available: https://dx.doi.org/10.1088/1361-6560/ab87f9

[5] F. Loignon-Houle, M. Toussaint, E. Bertrand, F. C. Lemyre, and R. Lecomte, "Timing estimation and limits in TOF-PET detectors producing prompt photons," *IEEE Trans. Radiat. Plasma Med. Sci.*, vol. 7, no. 7, pp. 692–703, Sep. 2023.

[6] M. Piller et al., "Performance evaluation of the FastIC readout ASIC with emphasis on cherenkov emission in TOF-PET," *Phys. Med. Biol.*, vol. 69, no. 11, May 2024, Art. no. 115014. [Online]. Available: https://dx.doi.org/10.1088/1361-6560/ad42fe

[7] M. Jacquet et al., "A high sensitivity cherenkov detector for prompt gamma timing and time imaging," *Sci. Rep.*, vol. 13, p. 3609, Mar. 2023. [Online]. Available: https://doi.org/10.1038/s41598-023-30712-x

[8] L. Rebolo et al., "Cherenkov light emission in pure cherenkov emitters for prompt gamma imaging," *IEEE Trans. Radiat. Plasma Med. Sci.*, vol. 8, no. 1, pp. 15–20, Jan. 2024.

[9] J. Ellin, L. Rebolo, M. Backfish, E. Prebys, and G. Ariño-Estrada, "Prompt gamma timing for proton range verification with TlBr and TlCl as pure cherenkov emitters," *Phys. Med. Biol.*, vol. 69, no. 11, May 2024, Art. no. 115002. [Online]. Available: https://dx.doi.org/10.1088/1361-6560/ad4304

[10] G. Ariño-Estrada et al., "Study of Čerenkov light emission in the semiconductors TlBr and TlCl for TOF-PET," *IEEE Trans. Radiat. Plasma Med. Sci.*, vol. 5, no. 5, pp. 630–637, Sep. 2021.

[11] N. Kratochwil, "Studies on time resolution for TOF-PET imaging utilizing cherenkov emission," Ph.D. dissertation, Fac. Phys., Univ. Vienna, Vienna, VA, Austria, 2023. [Online]. Available: https://ubdata.univie.ac.at/AC17016986

[12] (Nat. Inst. Stand. Technol., Gaithersburg, MD, USA). *National Institute of Standards and Technology, Database for Photon Cross Section*. Accessed: Nov. 23, 2023. [Online]. Available: https://physics.nist.gov/PhysRefData/Xcom/html/xcom1.html

[13] N. Kratochwil, S. Gundacker, and E. Auffray, "A roadmap for sole cherenkov radiators with SiPMs in TOF-PET," *Phys. Med. Biol.*, vol. 66, Sep. 2021, Art. no. 195001. [Online]. Available: https://dx.doi.org/10.1088/1361-6560/ac212a

[14] G. Terragni et al., "Time resolution studies of thallium based cherenkov semiconductors," *Front. Phys.*, vol. 10, Mar. 2022, Art. no. 785627. [Online]. Available: https://doi.org/10.3389/fphy.2022.785627

[15] G. Razdevšek et al., "Exploring the potential of a cherenkov TOF PET scanner: A simulation study," *IEEE Trans. Radiat. Plasma Med. Sci.*, vol. 7, no. 1, pp. 52–61, Jan. 2023.

[16] S. Gundacker, R. M. Turtos, E. Auffray, M. Paganoni, and P. Lecoq, "High-frequency SiPM readout advances measured coincidence time resolution limits in TOF-PET," *Phys. Med. Biol.*, vol. 64, no. 5, Feb. 2019, Art. no. 55012. [Online]. Available: https://dx.doi.org/10.1088/1361-6560/aafd52

[17] J. W. Cates and W.-S. Choong, "Low power implementation of high frequency SiPM readout for cherenkov and scintillation detectors in TOF-PET," *Phys. Med. Biol.*, vol. 67, no. 19, Sep. 2022, Art. no. 195009. [Online]. Available: https://dx.doi.org/10.1088/1361-6560/ac8963

[18] L. M. Bollinger and G. E. Thomas, "Measurement of the time dependence of scintillation intensity by a delayed-coincidence method," *Rev. Sci. Instrum.*, vol. 32, no. 9, pp. 1044–1050, Dec. 2004. [Online]. Available: https://doi.org/10.1063/1.1717610

[19] S. Gundacker, E. Auffray, K. Pauwels, and P. Lecoq, "Measurement of intrinsic rise times for various L(Y)SO and LuAG scintillators with a general study of prompt photons to achieve 10 ps in TOF-PET," *Phys. Med. Biol.*, vol. 61, no. 7, p. 2802, Mar. 2016. [Online]. Available: https://dx.doi.org/10.1088/0031-9155/61/7/2802

[20] S. Gundacker, R. M. Turtos, E. Auffray, and P. Lecoq, "Precise rise and decay time measurements of inorganic scintillators by means of X-ray and 511 keV excitation," *Nucl. Instrum. Methods Phys. Res. Sect. A, Accel., Spectrom., Detect. Assoc. Equip.*, vol. 891, pp. 42–52, May 2018. [Online]. Available: https://www.sciencedirect.com/science/article/pii/S0168900218302286

[21] R. Cala et al., "Characterization of mixed BGSO for crystal calorimetry at future colliders," *Nucl. Instrum. Methods Phys. Res. Sect. A, Accel., Spectrom., Detect. Assoc. Equip.*, vol. 1032, Mar. 2022, Art. no. 166527. [Online]. Available: https://www.sciencedirect.com/science/article/pii/S0168900222001334

[22] P. A. Čerenkov, "Visible radiation produced by electrons moving in a medium with velocities exceeding that of light," *Phys. Rev.*, vol. 52, pp. 378–379, Aug. 1937. [Online]. Available: https://link.aps.org/doi/10.1103/PhysRev.52.378

[23] I. Frank and I. Tamm, *Coherent Visible Radiation of Fast Electrons Passing Through Matter*. Berlin, Germany: Springer, 1991, pp. 29–35. [Online]. Available: https://doi.org/10.1007/978-3-642-74626-0_2

[24] H. Schröter, "Über die Brechungsindizes einiger Schwermetallhalogenide im Sichtbaren und die Berechnung von Interpolationsformeln für den Dispersionsverlauf," *Zeitschrift für Physik*, vol. 67, pp. 24–36, Jan. 1931. [Online]. Available: https://doi.org/10.1007/BF01391040

[25] (Nat. Inst. Stand. Technol., Gaithersburg, MD, USA). *National Institute of Standards and Technology, Stopping-Power and Range Tables for Electrons*. Accessed: Dec. 11, 2023. [Online]. Available: https://physics.nist.gov/PhysRefData/Star/Text/ESTAR-u.html

[26] "Low breakdown voltage type MPPC for scintillation detector," Data Sheet S14160, Hamamatsu, Shizuoka, Japan, Accessed: Jan 1, 2024. [Online]. Available: https://www.hamamatsu.com/content/dam/hamamatsu-photonics/sites/documents/99_SALES_LIBRARY/ssd/s14160_s14161_series_kapd1064e.pdf

[27] N. Kratochwil, E. Auffray, and S. Gundacker, "Exploring cherenkov emission of BGO for TOF-PET," *IEEE Trans. Radiat. Plasma Med. Sci.*, vol. 5, no. 5, pp. 619–629, Sep. 2021.

[28] S. Gundacker et al., "State of the art timing in TOF-PET detectors with LuAG, GAGG and L(Y)SO scintillators of various sizes coupled to FBK-SiPMs," *J. Instrum.*, vol. 11, no. 8, Aug. 2016, Art. no. P08008. [Online]. Available: https://dx.doi.org/10.1088/1748-0221/11/08/P08008

[29] R. H. Pots, "Investigation of new technologies to improve light collection from scintillating crystals for fast timing," Ph.D. dissertation, Fakultät für Mathematik, Informatik und Naturwissenschaften, RWTH Aachen University, Aachen, Germany, 2022. [Online]. Available: https://publications.rwth-aachen.de/record/846790

[30] J. Maebe and S. Vandenberghe, "Effect of detector geometry and surface finish on cerenkov based time estimation in monolithic BGO detectors," *Phys. Med. Biol.*, vol. 68, no. 2, Jan. 2023, Art. no. 25009. [Online]. Available: https://dx.doi.org/10.1088/1361-6560/acabfd

[31] S. Vinogradov, "Approximations of coincidence time resolution models of scintillator detectors with leading edge discriminator," *Nucl. Instrum. Methods Phys. Res. Sect. A, Accel., Spectrom., Detect. Assoc. Equip.*, vol. 912, pp. 149–153, Dec. 2018. [Online]. Available: https://www.sciencedirect.com/science/article/pii/S0168900217311956

[32] "NUV-HD single silicon photo multiplier," Data Sheet AFBR-S4N44C013, Broadcom Inc., San Jose, CA, USA. Accessed: Jan. 2, 2024. [Online]. Available: https://docs.broadcom.com/doc/AFBR-S4N44C013-DS

[33] D. R. Schaart, G. Schramm, J. Nuyts, and S. Surti, "Time of flight in perspective: Instrumental and computational aspects of time resolution in positron emission tomography," *IEEE Trans. Radiat. Plasma Med. Sci.*, vol. 5, no. 5, pp. 598–618, Sep. 2021.

[34] M. Yi, G. B. Ko, and J. S. Lee, "Pushing the limit of BGO-based dual-ended cherenkov PET detectors through photon transit time correction," *Phys. Med. Biol.*, vol. 69, no. 2, Jan. 2024, Art. no. 25005. [Online]. Available: https://dx.doi.org/10.1088/1361-6560/ad1549

[35] N. Kratochwil, E. Roncali, J. Cates, and G. Arino-Estrada, "High-performance dual-ended SiPM readout for TOF-PET with BGO and LYSO:ce," *IEEE Trans. Radiat. Plasma Med. Sci.*, 2024.

[36] M. S. Lee, J. W. Cates, A. Gonzalez-Montoro, and C. S. Levin, "High-resolution time-of-flight PET detector with 100 ps coincidence time resolution using a side-coupled phoswich configuration," *Phys. Med. Biol.*, vol. 66, no. 12, Jun. 2021, Art. no. 125007. [Online]. Available: https://dx.doi.org/10.1088/1361-6560/ac01b5

[37] V. Nadig et al., "Scalable, time-of-flight and depth-of-interaction detector units for high-resolution PET systems," *IEEE Trans. Radiat. Plasma Med. Sci.*, vol. 8, no. 1, pp. 1–14, Jan. 2024.

[38] C. Trigila, N. Kratochwil, B. Mehadji, G. Ariño-Estrada, and E. Roncali, "Intercrystal optical crosstalk in radiation detectors: Monte carlo modeling and experimental validation," *IEEE Trans. Radiat. Plasma Med. Sci.*, vol. 8, no. 7, pp. 734–742, Sep. 2024.

[39] A. Mariscal-Castilla et al., "Toward sub-100 ps TOF-PET systems employing the FastIC ASIC with analog SiPMs," *IEEE Trans. Radiat. Plasma Med. Sci.*, vol. 8, no. 7, pp. 718–733, Sep. 2024.